Earth's Future

RESEARCH ARTICLE
10.1029/2022EF002790

Key Points:

- Reversal of surface air temperature (SAT) anomalies between early and late winter is an intrinsic feature of the Arctic-Eurasian climate
- The changes of Ural blocking in late December may indicate whether the SAT in late winter will be reversed to early winter
- Robust climate dynamic processes associated with such a reversal of SAT are found in both reanalysis data and long-term model simulations

Supporting Information:

Supporting Information may be found in the online version of this article.

Correspondence to:

S. He,
Shengping.He@uib.no

Citation:

Xu, X., He, S., Zhou, B., & Wang, H. (2022). Atmospheric contributions to the reversal of surface temperature anomalies between early and late winter over Eurasia. *Earth's Future*, *10*, e2022EF002790. https://doi.org/10.1029/2022EF002790

Received 21 MAR 2022
Accepted 15 AUG 2022

Atmospheric Contributions to the Reversal of Surface Temperature Anomalies Between Early and Late Winter Over Eurasia

Xinping Xu[1], Shengping He[2,3,4], Botao Zhou[1], and Huijun Wang[1,4,5]

[1]Collaborative Innovation Center on Forecast and Evaluation of Meteorological Disasters/Key Laboratory of Meteorological Disaster, Ministry of Education, Nanjing University of Information Science and Technology, Nanjing, China, [2]Geophysical Institute, University of Bergen and Bjerknes Centre for Climate Research, Bergen, Norway, [3]Nansen Environmental and Remote Sensing Center and Bjerknes Centre for Climate Research, Bergen, Norway, [4]Nansen-Zhu International Research Center, Institute of Atmospheric Physics, Chinese Academy of Sciences, Beijing, China, [5]Southern Marine Science and Engineering Guangdong Laboratory (Zhuhai), Zhuhai, China

Abstract Observations have shown subseasonal reversal of temperature anomalies between early and late winter over Eurasia, which is distinct from the seasonal mean condition. Based on the reanalysis data, the 1800-year control simulation and the 40-member ensemble simulations in 1920–2100 from the Community Earth System Model (CESM) Large Ensemble (CESM-LE), this study reveals that the reversal of surface air temperature (SAT) anomalies between early and late winter is one of the dominant and intrinsic features of the Arctic-Eurasian winter climate. Such a reversal is characterized by "colder Arctic, warmer Eurasia" in December (January–February) and "warmer Arctic, colder Eurasia" in January–February (December). Robust climate dynamic processes associated with the reversal of SAT anomalies, including subseasonal reversals of anomalies in the Ural blocking, midlatitude westerlies, and stratospheric polar vortex, are found in both reanalysis data and CESM simulations, indicating the important role of internal atmospheric variability. Further analysis reveals that the reversal of Ural blocking anomalies in late December can be a potential precursor for the reversal of SAT anomalies in late winter. The reversal of midlatitude westerly wind anomalies associated with the Ural blocking can affect upward propagation of planetary-scale waves especially with wavenumber 1, subsequently promoting the contribution of stratospheric polar vortex to the reversal of SAT anomalies in late winter over the Arctic-Eurasian regions. Such a troposphere-stratosphere pathway triggered by the perturbation of tropospheric circulations is confirmed by the CESM-LE simulations, and it may be useful for the prediction of subseasonal reversal of SAT anomalies.

Plain Language Summary Observations show that Eurasia may experience subseasonal reverse temperature anomalies from early to late winter. For example, the warmer-than-normal conditions in early winter can change to colder-than-normal conditions in late winter. Such a reverse temperature anomaly in Eurasia is usually concurrent with a reverse one in the Arctic. The "colder Arctic, warmer Eurasia" pattern in early winter followed by "warmer Arctic, colder Eurasia" pattern in late winter is robustly detected in climate model simulations, indicating that the subseasonal reversal of temperature anomalies is one of the intrinsic features of the Arctic-Eurasian climate. This feature is associated with robust climate dynamic processes, including subseasonal reversals of the anomalies in the Ural blocking, the midlatitude westerly winds, and the stratospheric polar vortex. Because the Ural blocking can trigger the troposphere-stratosphere interaction, the reversal of Ural blocking anomalies in late December can be a potential precursor for the reversal of surface air temperature anomalies in late winter.

1. Introduction

East Asia frequently experiences cold surges in winter and has lower temperatures than Europe at the same latitude. Frigid temperatures gripping East Asia are often triggered by abnormally strong East Asian winter monsoon (EAWM) which is known as one of the most active climate systems in boreal winter (Miao et al., 2019; Tao & Chen, 1987). Previous studies have indicated that the interannual variability of the EAWM is closely associated with El Niño-Southern Oscillation (ENSO) (Wang & He, 2012; B. Wang et al., 2000; Y. Zhang et al., 1997). It has also been documented that changes in the Arctic properties (such as Arctic sea ice loss and Arctic warming) (Gao

et al., 2015; S. Li et al., 2018; Liu et al., 2012; Mori et al., 2019; Wang & Liu, 2016; H. Wang et al., 2015) and high-latitude Eurasian snow cover (J. L. Cohen et al., 2012; Furtado et al., 2015; Orsolini & Kvamstø, 2009; Xu, He, et al., 2018) may have significant influences on the climate over the downstream East Asia through inducing a distinct thermal and dynamical teleconnection. Most of these studies have focused on seasonal mean conditions, while more and more studies emphasized that the teleconnections on the monthly time scale are different to the seasonal mean (He & Wang, 2013; King et al., 2018, 2021).

Recent observations indicate that early and late winter climate anomalies can abnormally display an out-of-phase pattern on the subseasonal timescale. For example, winter 2014/2015 was colder than normal in East Asia in December 2014 but a milder condition occurred in January and February 2015 (Xu, Li, et al., 2018). Reduced Arctic sea ice in conjunction with warm tropical sea surface temperature (SST) anomalies under the positive phase of the Pacific Decadal Oscillation are hypothesized to play a major role in the relevant processes (Xu, Li, et al., 2018). Moreover, despite the warmer-than-normal temperatures in December 2015, an extreme cold surge hit East Asia in January 2016, causing record-breaking low temperatures and anomalously large snowfall (Geng et al., 2017). Cheung et al. (2016) attributed such an extremely cold event in January 2016 to the subseasonal phase transition of the Arctic Oscillation (AO) which shifted from strong positive phase in December to negative phase in January. The important role of the super El Niño event was also discussed (Geng et al., 2017; G. Zhang et al., 2019). He et al. (2016) concluded that the super El Niño in combination with the unprecedented Arctic warming led to the severe cold January of 2016. It is worth noting that a record-breaking Arctic warming event occurred in January 2016 (Kim et al., 2017) before the record-breaking cold surge that swept across East Asia.

The Arctic has been warming dramatically since the 1990s with a rate of about 2–3 times that of the global mean, which is referred to as the Arctic amplification (Cowtan & Way, 2013; Screen, 2017; Screen & Simmonds, 2010). Concurrent with the rapid Arctic warming, Eurasia has experienced more frequent cold winters and a pronounced cooling trend during 1990–2013 (J. Cohen et al., 2014), forming the warm Arctic-cold Eurasia (WACE) pattern (J. E. Overland et al., 2011). A novel set of observational and modeling studies have focused on the linkage between Arctic warming and midlatitude climate (Gao et al., 2015; Kug et al., 2015; Luo et al., 2016; J. Overland et al., 2015). Recent studies (e.g., He et al. (2020) and Labe et al. (2020)) revealed that the different vertical extension of Arctic warming upward the troposphere is closely related to the difference among climate models in simulating the WACE pattern. Nonetheless, the mechanism for the linkage between Arctic warming and subseasonal variability of East Asian surface air temperature (SAT), especially the out-of-phase SAT anomalies pattern between early and late winter, still remains unclear.

The reoccurrence of subseasonal reversals in the sign of climate anomalies in recent decades has been attributed to changes in tropical Pacific SST (H. Li et al., 2021) and Arctic sea ice (Dai et al., 2019), yet the impact of Arctic sea ice loss on the midlatitude climate remains a controversial issue (J. Cohen et al., 2020; Screen et al., 2018). In this study, we present robust evidence to demonstrate that the subseasonal reversal from warm anomalies in early winter to cold anomalies in late winter over Eurasia (including East Asia) is closely associated with the reversal from cold anomalies in early winter to warm anomalies in late winter over the Barents-Kara Seas. The key advance of this study is that a troposphere-stratosphere pathway is revealed, which can be used to predict the reversal of SAT anomalies in late winter.

2. Data and Methods

Monthly and daily atmospheric data sets including SAT, sea level pressure (SLP), wind field at 850 hPa (UV850), turbulent heat flux, air temperature, geopotential height, zonal wind, and specific humidity are obtained from the European Centre for Medium-Range Weather Forecasts (ECMWF) Interim Reanalysis (ERA-I; 1979–2019), with a horizontal resolution of 1.0° × 1.0° (Dee et al., 2011). Monthly atmosphere data sets from ECMWF Twentieth Century Reanalysis (ERA20C; 1900–2010) are also examined (Poli et al., 2016) to support the results derived from ERA-I. Monthly sea ice concentration is obtained from the Met Office Hadley Center (Rayner et al., 2003). These data are linearly detrended. In addition, a 15-day low-pass filter is applied to daily data.

A 1800-year preindustrial control (PiCTL) simulation and 40-member ensemble of historical simulations (1920–2005) and future projections (2006–2100) from the Community Earth System Model (CESM) Large Ensemble (CESM-LE) are employed (Kay et al., 2015) to support the results and mechanisms obtained from the short-term (40 years) reanalysis data. The 1800-year PiCTL simulation is forced by the non-evolving

Table 1
The Correlation Coefficients of East Asian Surface Air Temperature Index (EATI_2m) Between Different Winter Months From December to February During 1979/1980–2018/2019

	December	January	February
December	1		
January	0.193	1	
February	0.258	0.496***	1
January–February	0.263	0.844***	0.884***

Note. *** Indicates that the correlation coefficients are significant at 99% confidence level.

preindustrial condition. The historical simulations and future projections are conducted using the fully coupled CESM model. Each ensemble member is subject to identical radiative forcing of greenhouse gases (historical forcing in 1920–2005 and future representative concentration pathway 8.5 in 2006–2100) but with a small (order of 10^{-14} K) random noise perturbation to their initial atmospheric temperature fields. We have removed the least squares quadratic trend from the outputs of CESM simulations before any analysis; variables including SAT, SLP, air temperature, geopotential height, and meridional and zonal wind with a horizontal resolution of 0.9° latitude × 1.25° longitude are analyzed.

The East Asian surface temperature index (EATI_2m) is defined as area-averaged SAT in the domain (35°N–50°N, 80°E–130°E) (Kug et al., 2015). The Arctic surface temperature index (ARTI_2m) and midtropospheric temperature index (ARTI_500) are, respectively, defined as the area-averaged SAT and 500 hPa air temperature over the Barents-Kara Seas (70°N–80°N, 30°E–70°E; black frame in Figure 2b) (He et al., 2020). Applying the empirical orthogonal function (EOF) analysis to the SAT over Eurasia (20°N–90°N, 0°E–180°E) for the period of 1979/1980–2018/2019, we define the second principal component time series as the WACE index, following the study of Sung et al. (2018). The instantaneous blocking (IB) index is defined as the sum of IB events (Tibaldi & Molteni, 1990) from 0° to 120°E. All indices are normalized. The standard two-tailed Student's *t* test is implemented for significance test in this study.

We use the Eliassen-Palm (E-P) flux (Andrews et al., 1987) to diagnose the planetary wave activity propagation: $F(\varphi) = -\rho r\cos\varphi\overline{u'v'}$ and $F(p) = \rho r\cos\varphi(\overline{\theta'v'}/\overline{\theta_p})$, where φ is the latitude, ρ is the air density, r is the mean radius of the earth, u is the zonal wind, v is the meridional wind, p is the pressure, θ is the potential temperature, and $\theta_p = d\theta/dp$.

In this study, winter refers to the months of December in the current year (early winter) and January and February (late winter) in the subsequent year. The division of early and late winter is based on the statistical analysis results of ERA-I: (a) significant high correlation between January and February EATI_2m that show a consistent sign in 27 out of 40 winters (67.5%), and (b) insignificant correlation between December and January (January–February mean) EATI_2m (Table 1). Two categories of winter are identified in this study, which are referred to as warm-to-cold (cold-to-warm) winters characterized by warmer (colder) early winter and colder (warmer) late winter over East Asia. Warm-to-cold (cold-to-warm) winters are identified when the difference in the normalized EATI_2m between early and late winter is above 1.0 (below −1.0). Ten (i.e., ∼25%) warm-to-cold winters (1979, 1983, 1987, 1989, 1999, 2004, 2007, 2011, 2015, and 2017) and nine (i.e., ∼23%) cold-to-warm winters (1981, 1984, 2001, 2002, 2005, 2006, 2012, 2014, and 2018) are identified (Figure 1). Note that the composite results are not sensitive to the thresholds used for identifying warm-to-cold (cold-to-warm) winters in reanalysis data and CESM simulations.

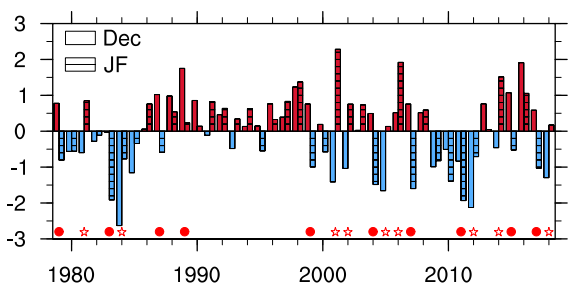

Figure 1. Normalized time series of the December and January–February mean EATI_2m during 1979/1980–2018/2019 from ERA-I. The dots (stars) indicate winters when the difference between December (i.e., early winter) and January–February mean (i.e., late winter) normalized EATI_2m is above 1.0 (below −1.0).

3. Results

3.1. Subseasonal Reversal of SAT Anomalies Over the Arctic-Eurasian Regions

Figure 2 displays composite differences of atmospheric fields in December and January–February between warm-to-cold and cold-to-warm winters during 1979/1980–2018/2019. In December, large positive temperature differences are observed not only in East Asia (e.g., east of ∼100°E) but also in the Eurasian continent from 40°N to 65°N (Figure 2a; shading). The difference can reach up to 6°C in Siberia (Figure 2a; shading). These warmer conditions, however, are replaced by significant colder conditions in the subsequent January–February that cover the broad area from Siberia to East Asian coast (Figure 2b; shading). Meanwhile, positive temperature differences emerge in the Arctic with the maximum value of more than 6°C located at the Barents-Kara Seas (Figure 2b; shading). The contrasting SAT

10.1029/2022EF002790

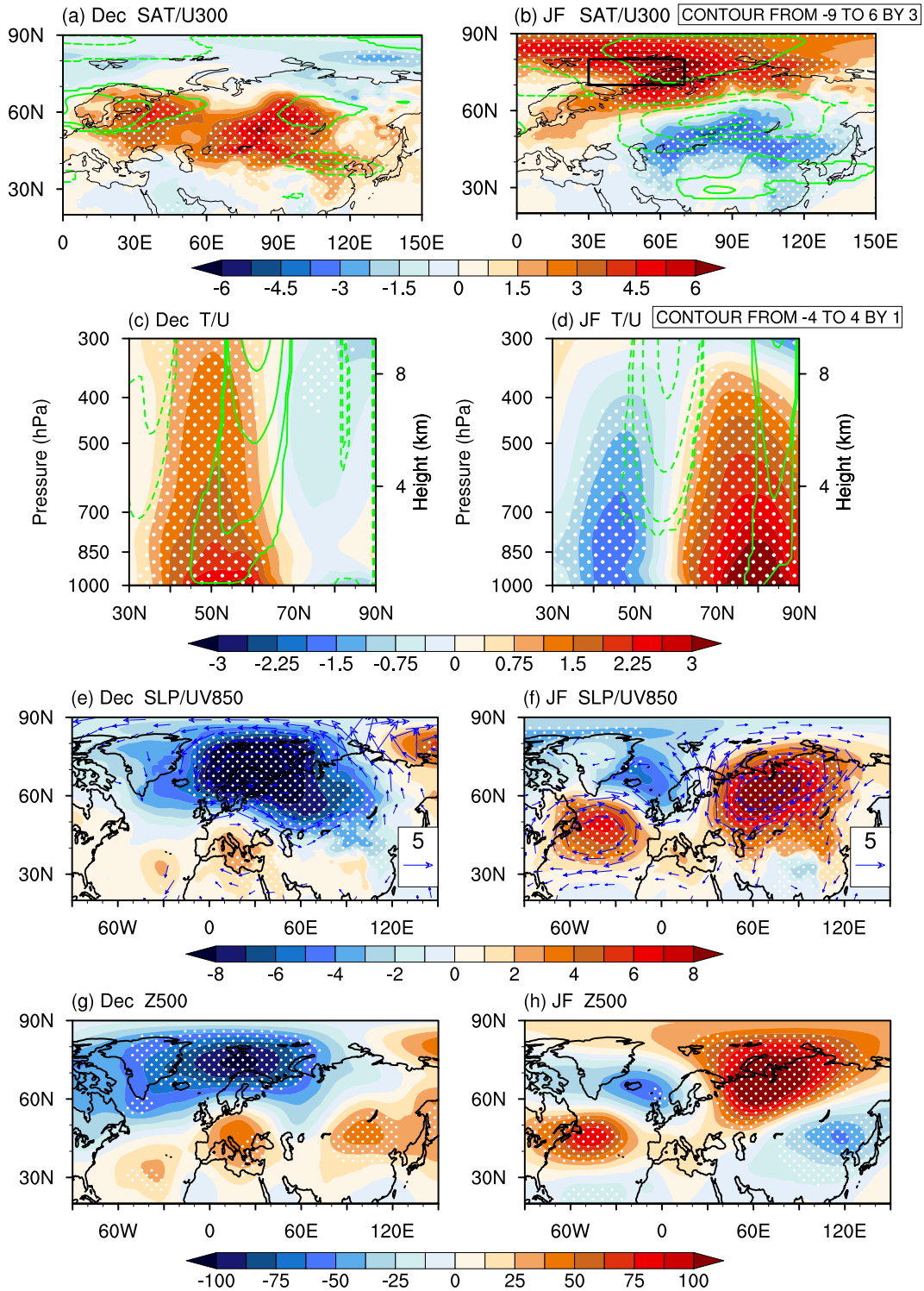

Figure 2. Differences of (a) December and (b) January–February mean surface air temperature (SAT; shading; units: °C) and 300 hPa zonal wind (U300) (contours; units: m s^{-1}) anomalies composited between warm-to-cold and cold-to-warm winters over East Asia during 1979/1980–2018/2019 obtained from ERA-I. (c–f) Same as (a and b), but for (c and d) vertical temperature (shading; units: °C) and zonal wind (contours; units: m s^{-1}) averaged along 0°E–150°E, (e, f) sea level pressure (SLP; shading; units: hPa) and wind field at 850 hPa (UV850) (vectors; units: m s^{-1}), and (g, h) 500 hPa geopotential height (Z500) (units: m). Regions with significant anomalies above the 90% confidence level are marked with dots. The contours and vectors are displayed only if the corresponding anomalies exceed the 90% confidence level.

anomalies between the Arctic and Eurasia shown in Figure 2b bear a high similarity to the WACE pattern. In the vertical direction, strong warm and cold anomalies in late winter can extend to the upper troposphere, forming the deep Arctic warming-colder Eurasia pattern (Figure 2d; shading) as proposed by He et al. (2020). At the same time, accompanied with the deep Arctic warming and colder Eurasia, the tropospheric zonal winds markedly decelerate across northern Eurasia (45°N–65°N, 0°E–150°E) (Figures 2b and 2d; contours). An opposite pattern in the vertical direction is revealed in December, though Arctic cold anomalies are less significant (Figure 2c). In the SLP field, a cyclonic anomaly stretches from the Arctic to Siberia in early winter, which is replaced by an anticyclonic anomaly over Eurasia in late winter when the North Atlantic Oscillation (NAO) enters a positive phase (Figures 2e and 2f). The mid-tropospheric Ural blocking changes from a weakened state in early winter to a strengthened one in late winter, concurrent with reverse changes in the East Asian trough (Figures 2g and 2h). The evolutions of the climate anomalies described above are largely symmetric between warm-to-cold composites and cold-to-warm composites (Figures S1 and S2 in Supporting Information S1). Note that the missing of significant cold anomalies over the Barents-Kara Seas (Figure 2a and Figure S1a in Supporting Information S1) is attributed to the limited sample size in the short ERA-I reanalysis record. We have repeated the analysis using the long-term reanalysis data (i.e., ERA20C), which can provide more samples (i.e., twenty-six warm-to-cold cases and twenty-five cold-to-warm cases). Clear symmetric anomaly patterns between early and late winter have been illustrated by the ERA20C data (Figures S3–S5 in Supporting Information S1). It has been argued that the anomalous anticyclone in the high latitude can promote warm and moist air transport from lower latitudes into the Barents-Kara Seas (McCusker et al., 2016), or be influenced by Arctic warming and cause cold air advection from the Arctic to Eurasia (Kug et al., 2015). The above analysis has shown that the subseasonal out-of-phase temperature anomalies over Eurasia and the Arctic are closely associated with the subseasonal out-of-phase large-scale atmospheric circulation anomalies. However, we here cannot determine the direction of causality.

To reveal how climate anomalies evolve from early to late winter, we examine temporal evolutions of composite daily SAT anomalies between warm-to-cold and cold-to-warm winters (Figures 3a and 3b). As shown in Figure 3a, the SAT anomaly at the warm center over central Eurasia (60°E–120°E) reaches 6°C during the first half of December. It then tends to be weaker and less significant and becomes negative at around 1st January. A strong cold center (with SAT anomaly below −6°C) dominates central Eurasia from mid-January to mid-February (Figure 3a). It implies that the subseasonal reversal of SAT anomalies over Eurasia recorded in the monthly mean data set can be further confirmed by the results on the synoptic time scale. Interestingly, the midlatitude warm center starts moving northward since the second half of December and a pronounced warming occurs in the Barents-Kara Seas in late December (Figure 3b). Moreover, the occurrence of Arctic warm anomalies precedes Eurasian cold anomalies in early January (Figure 3b). Figure 3c further illustrates the corresponding temporal evolutions of the normalized daily EATI_2m, ARTI_2m, and ARTI_500 from 1st December to 28th February. As expected, the Arctic surface and mid-troposphere uniformly switch from anomalously cold state to anomalously warm state in mid-December, and significant warm anomalies further develop there in late winter (Figure 3c). Following the warmer Arctic, East Asia becomes significantly colder in late winter (Figure 3c). The synoptical-scale results further suggest that the shift from warm to cold anomalies in Eurasia is preceded by the shift from cold to warm anomalies in the Arctic. Such a lead-lag relationship (Figure 3c) might indicate the potential impact of deep Arctic warming on the presence of Eurasian cold anomalies, given that the deep Arctic warming may decelerate the midlatitude westerly winds by weakening the poleward temperature gradient (He et al., 2020; Ye et al., 2018). Additionally, other forcing factors may lead to the exceptional cases where there is no reversal of SAT anomalies between late December and early January (Figure 3c). We now could not rule out the possibility that both the deep Arctic warming and Eurasian cold anomalies are induced by the same atmospheric circulation patterns such as the Ural blocking and the polar vortex. We will address this question in the following section.

3.2. Mid- and High-Latitude Atmospheric Circulation Changes Responsible for the Reversal of Both Arctic and Eurasian Temperature Anomalies

Synoptic storm tracks from the North Atlantic to the Arctic (He et al., 2020; Kim et al., 2017) and an internally generated atmospheric circulation pattern (Luo et al., 2016; McCusker et al., 2016) may cause both anomalous warming in the Arctic and cold anomalies over Eurasia. It is worth noting that the January–February mean Ural pressure ridge is significantly reinforced relative to that in December (Figures 2g and 2h). To corroborate the lead-lag relationship between atmospheric circulation variability and temperature anomalies, we examine the

10.1029/2022EF002790

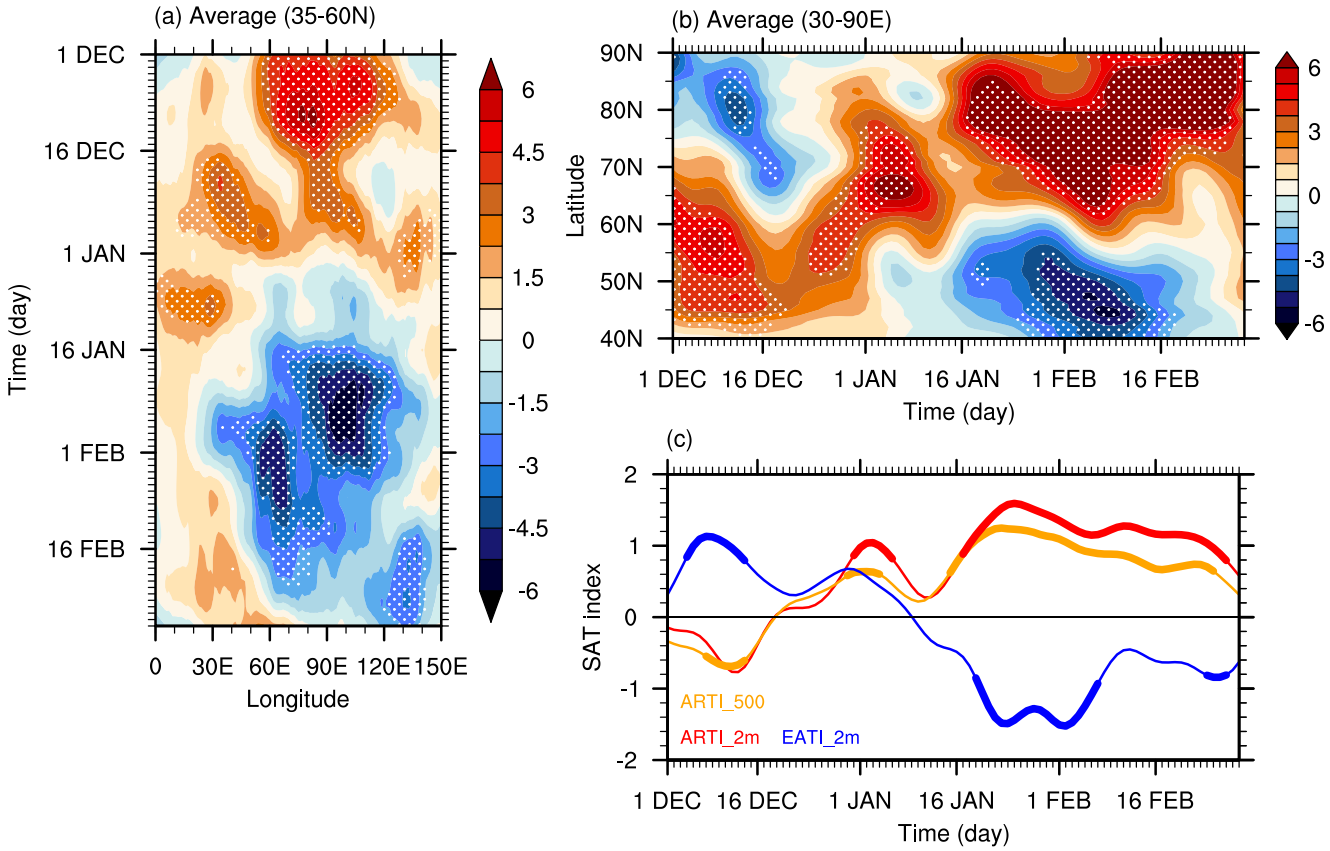

Figure 3. Differences of (a) the meridional-mean surface air temperature (SAT) anomalies (units: °C) along 35°N–60°N, (b) the zonal-mean SAT anomalies (units: °C) along 30°E–90°E, (c) normalized EATI_2m, ARTI_2m, and ARTI_500 evolving from 1 December to 28 February (15-day low-pass-filtered) composited between warm-to-cold and cold-to-warm winters over East Asia during 1979/1980–2018/2019 obtained from ERA-I. (a, b) Regions with significant anomalies above the 90% confidence level are marked with dots. Thick curves in (c) indicate the values exceeding the 90% confidence level.

temporal evolution of composite IB index and WACE index (Figure 4). On the daily time scale, a rapid transition of the IB index from negative to positive occurs in mid-December (Figure 4). The presence of more frequent IB events over northern Eurasia in late December precedes the WACE pattern that emerges in early January (Figure 4). This result indicates the possible influence of Ural blocking development on the reversal of SAT anomalies from early winter to late winter over the Arctic-Eurasian regions. As expected, the significant warm and moist air intrusion from lower latitudes into the Barents-Kara Seas in January–February promotes sea ice melt there (Figure S6 in Supporting Information S1) and increases temperature anomalies (Figure 2d; shading). The anomalous heat transfer from the atmosphere to the ocean (Figure S6 in Supporting Information S1) is indicative of the atmosphere-driven coupling (Blackport et al., 2019; Sorokina et al., 2016).

Considering that the atmospheric circulation variability is strongly related to stationary planetary wave activity (Andrews et al., 1987), we further examine the potential wave-mean flow interactions associated with the subseasonal temperature anomaly reversal. Figure 5 presents composite E-P flux and divergence (sum of wavenumber 1–3) of the planetary waves in early and late winter, and their differences. Anomalous downward propagation of planetary waves from the upper stratosphere to the troposphere is observed along the polar waveguide in early winter (Figure 5a; vectors). The weaker polar wave guide leads to anomalous E-P flux divergence in the upper troposphere (Figure 5a; 50°N–65°N, red contours), which consequently accelerates the westerly winds around 60°N (Figure 2c; contours) (Andrews et al., 1987; L. Wang et al., 2009). The vertical flux of wave activities from the troposphere is proportional to the strengthening of poleward eddy heat transport (Peings & Magnusdottir, 2014). The anomalous downward propagation of E-P flux anomalies in early winter (Figure 5a) implies a reduced upward flux of wave activities and therefore a reduced convergence of wave activities in the polar vortex region, indicating a strengthened stratosphere polar vortex. The situation is opposite in late winter (Figure 5b). Enhanced vertical wave activities in late winter imply increased convergence of wave activities in the polar vortex region

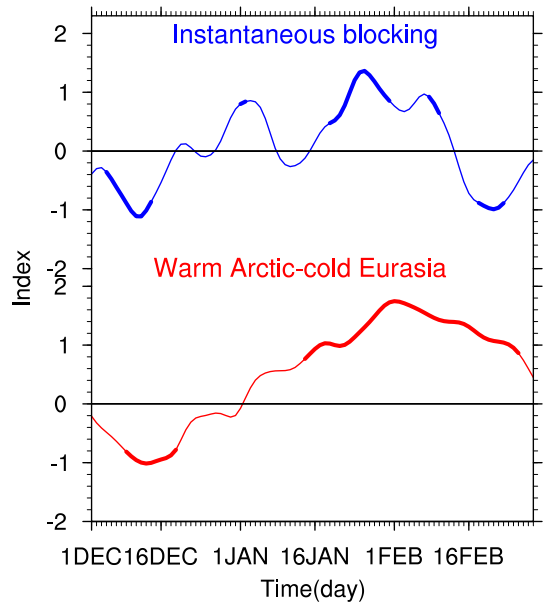

Figure 4. Differences of the normalized instantaneous blocking index and warm Arctic-cold Eurasia index from 1 December to 28 February (with 15-day low-pass-filtered) composited between warm-to-cold and cold-to-warm winters over East Asia during 1979/1980–2018/2019 obtained from ERA-I. Thick curves indicate the values exceeding the 90% confidence level.

and more poleward eddy heat transport (Figures 5b and 5c), which causes a weakened vortex. It is thus revealed that the subseasonal reversal in stratospheric polar vortex anomalies may play an important role in fueling the reversal of Eurasian climate anomalies. Note that the enhanced vertical wave activities in late winter (Figure 5b; vectors) may be caused by the reversal of tropospheric anomalies such as the strengthened Ural blocking that occurs in late December (Figure 4), because the weakened midlatitude westerly associated with the strengthened Ural blocking is favorable for the upward propagation of the stationary wave activities (Dickinson, 1968).

In this section, we propose that the subseasonal reversal of temperature anomalies from early winter to late winter could be attributed to changes in mid- and high-latitude atmospheric circulation patterns such as the Ural blocking and the stratospheric polar vortex. A more detailed discussion based on model simulations will be elucidated next.

3.3. Results From CESM PiCTL and CESM-LE Simulations

There exists a substantial degree of internal atmospheric variability that is intrinsic at mid- and high-latitudes (Vavrus, 2018). The 1800-year CESM PiCTL and large ensemble CESM-LE simulations are employed to verify the robust role of internal atmospheric variability (Deser et al., 2016) in leading to subseasonal reversals of surface temperature anomalies over the Arctic-Eurasian regions. In order to identify the contribution of internal variability to the occurrence of reversal events, variables from the CESM PiCTL simulation are first analyzed. Approximately 20% of the 1800 winters experience a warm-to-cold reversal over Eurasia and about 20% of the winters experience a cold-to-warm reversal, close to the sample proportions in observations. The composite temperature differences between warm-to-cold and cold-to-warm winters based on the PiCTL simulation (Figures 6a and 6b) are consistent with the observed results. Figure 6a shows a warm anomaly center in central Eurasia and a cold anomaly center in the Barents-Kara Seas in early winter (shading), which is followed by a reversed pattern in late winter (Figure 6b; shading). Note that the above anomalous temperature patterns can vertically extend to the upper troposphere (Figures 6c and 6d; shading). Correspondingly, the mid- and high-latitude (around 60°N) westerly winds circling the Arctic significantly accelerate (decelerate) in early (late) winter (Figures 6a–6d; contours). The SLP anomaly over northern Eurasia exhibits a clear change from an anomalous low center in

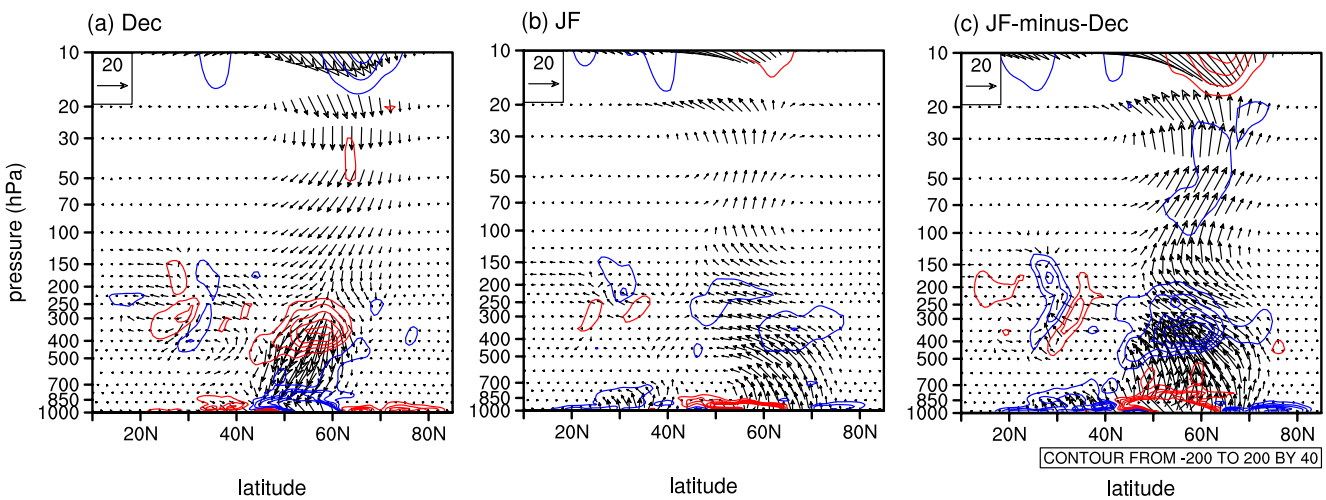

Figure 5. Differences of (a) December, (b) January–February mean, and (c) January–February mean minus December Eliassen-Palm (E–P) flux (vectors; units: 10^7 m^2 s^{-2}) as well as the corresponding divergence anomalies (contours; units: m s^{-1} day^{-1}; red/blue contours indicate anomalous divergence/convergence) composited between warm-to-cold and cold-to-warm winters over East Asia during 1979/1980–2018/2019 obtained from ERA-I.

10.1029/2022EF002790

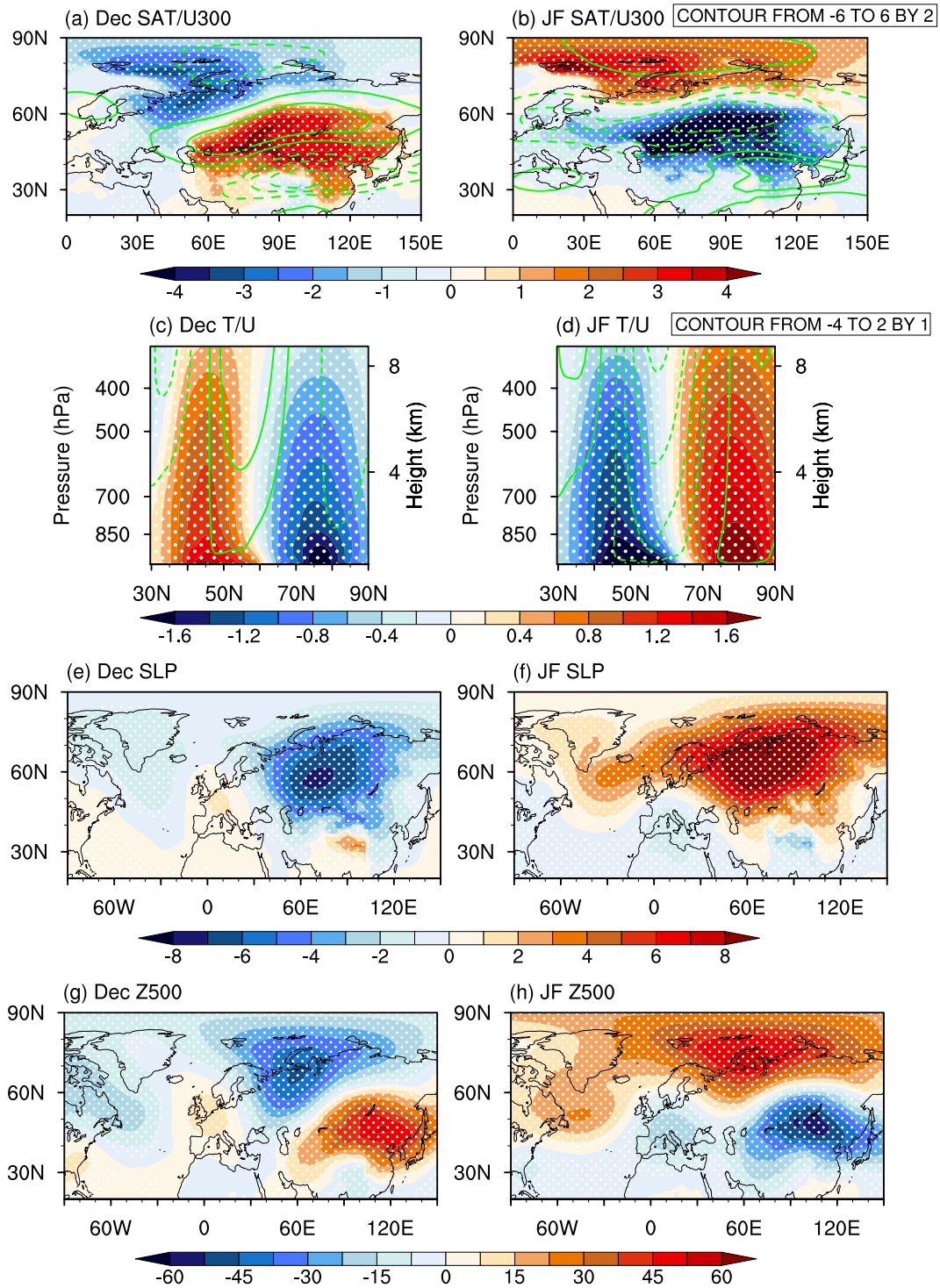

Figure 6. Differences of (a) December and (b) January–February mean surface air temperature (SAT; shading; units: °C) and U300 (contours; units: m s^{-1}) anomalies composited between warm-to-cold and cold-to-warm winters over East Asia based on the 1800-year Community Earth System Model preindustrial control simulation. (c–h) Same as (a and b), but for (c and d) vertical temperature (shading; units: °C) and zonal wind (contours; units: m s^{-1}) averaged along 0°E–150°E, (e, f) sea level pressure (SLP; units: hPa), and (g, h) Z500 (units: m). Regions with significant anomalies above the 95% confidence level are marked with dots. The contours are displayed only if the corresponding anomalies exceed the 95% confidence level.

10.1029/2022EF002790

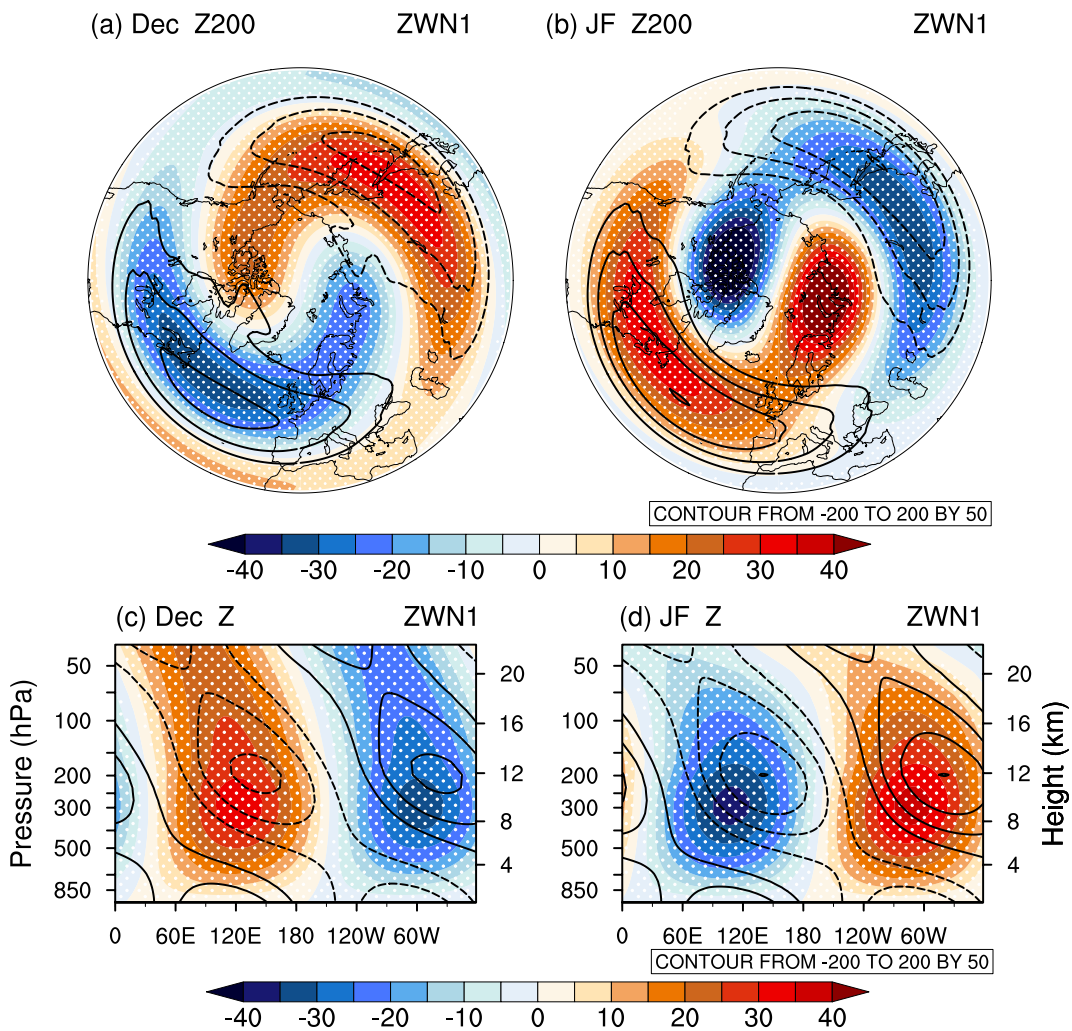

Figure 7. Differences of (a) December and (b) January–February mean zonal wave-number 1 component of 200 hPa geopotential height (Z200) (shading; units: m) composited between warm-to-cold and cold-to-warm winters over East Asia based on the 1800-year Community Earth System Model preindustrial control simulation. The composite differences (shading) are compared with the long-term climatology (contours). (c, d) Same as (a and b), but along the longitude-pressure section at 45°N. Regions with significant anomalies above the 95% confidence level are marked with dots.

early winter to an anomalous high center (i.e., a strengthened Ural blocking) in late winter (Figures 6e and 6f). In the mid-troposphere, the most prominent characteristic is the pronounced wave-like pattern composed of an enhanced pressure ridge near the Urals and a deepened trough over midlatitude Eurasia in late winter, which is completely reversed in early winter (Figures 6g and 6h). More broadly, we can see a reverse AO/NAO phase between early and late winter (Figures 6e–6h), which is highly consistent with that in ERA20C (Figures S3e–S3h in Supporting Information S1). The large samples from the 1800-year PiCTL simulation and the statistically significant composite anomalies (Figure 6) that closely resemble the results shown in observations (Figure 2 and Figure S3 in Supporting Information S1) further confirm that the subseasonal reversal of temperature anomalies over the Arctic-Eurasian regions between early and late winter is an intrinsic feature of the climate.

Moreover, the wave activities in the troposphere as well as stratosphere are largely determined by zonal wavenumber-1 component. As shown in Figure 7, the composite differences of wavenumber-1 component of geopotential height anomalies are tightly in (out of) phase with climatology in late (early) winter in both zonal and vertical directions. The wavenumber-1 that is in phase with the climatological planetary-scale wave in late winter will interfere with it, which may weaken the polar vortex (Kim et al., 2014). These results, which can also be detected in observations (Figure S7 in Supporting Information S1), further indicate that the perturba-

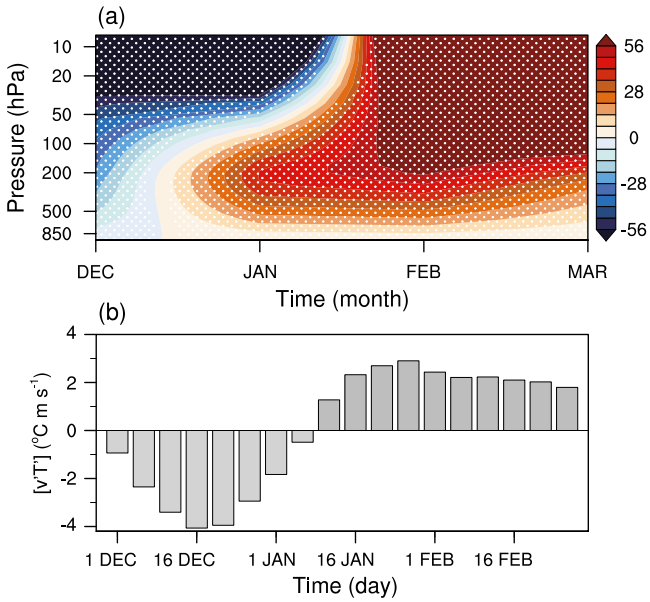

Figure 8. Differences of (a) monthly polar cap height anomaly (units: m) from December to March and (b) 5-day averaged poleward heat flux anomalies (units: °C m s^{-1}) at 200 hPa along 65°N from 1 December to 28 February (with 15-day low-pass-filtered) composited between warm-to-cold and cold-to-warm winters over East Asia during 1920/1921–2099/2100 based on 40 ensemble members of Community Earth System Model Large Ensemble. (a) Regions with significant anomalies above the 95% confidence level are marked with dots.

tion of tropospheric circulation might play an important role in triggering the troposphere-stratosphere interaction that eventually leads to the reversal of SAT anomalies between early and late winter over the Arctic-Eurasian regions.

It is worth noting that nearly identical results can also be found in the 40-member ensemble CESM-LE simulations spanning from 1920 to 2100 (Figures S8 and S9 in Supporting Information S1). Moreover, the sample proportion of reversal events in the large ensemble CESM-LE (7200 winters) is nearly equal to that in CESM PiCTL (i.e., ∼20% warm-to-cold reversals and ∼20% cold-to-warm reversals). This result further confirms that the subseasonal reversal of Eurasian temperature anomalies is primarily driven by internal atmospheric variability such as reversed changes in the Ural blocking. Given that the variability of the Ural blocking anomalies on the synoptic time scale may provide insights into predicting the reversal of SAT anomalies in late winter (e.g., Figure 4), we further investigate daily outputs from the CESM-LE simulations. Due to (a) the lack of daily data in CESM PiCTL and (b) the consistent results between PiCTL and CESM-LE, the analysis below is based on CESM-LE simulations.

To identify the potential causality between atmospheric circulation variabilities in the troposphere and stratosphere, we present temporal evolution of the composite differences of polar cap height (PCH) that measures the area-averaged geopotential height northward of 65°N from 1000 to 10 hPa. In December, negative PCH anomalies emerge throughout the troposphere and stratosphere, indicating a strengthened polar vortex (Figure 8a). The strengthened stratospheric polar vortex may lead to a positive AO phase in the troposphere (J. Cohen et al., 2014), which will induce positive near-surface temperature anomalies in central Eurasia (Figure 6a; shading) through modulating temperature advection (Huang et al., 2021). The most dramatic feature shown in Figure 8a is that the PCH anomalies reverse to significant positive ones in the subsequent January and February. Particularly, positive PCH anomalies first emerge in the troposphere from late December, then propagate upwards into the stratosphere and eventually lead to significant positive anomalies throughout the troposphere and stratosphere in late winter (Figure 8a). Positive PCH anomalies indicate a weakened polar vortex. The results imply that the tropospheric atmospheric circulation patterns such as stationary waves (Figure 7) could induce the reversed anomalies of the polar vortex, which can subsequently cause the reversal of temperature anomalies. A better understanding of the stratospheric polar vortex weakening triggered by tropospheric circulation variability can be obtained by computing poleward eddy heat flux, which quantifies the intensity of vertical wave activities (Polvani & Waugh, 2004). Figure 8b shows the associated 5-day averaged zonal mean eddy heat flux at 200 hPa along 65°N. Notable negative poleward heat flux anomalies appear in December (Figure 8b), consistent with the anomalous downward propagation of E-P flux detected in observations (Figure 5a). From mid-January, anomalous increased poleward eddy heat flux emerges and intensifies thereafter (Figure 8b), indicating increased vertical wave activities from the troposphere that weaken the stratospheric polar vortex. This analysis indicates that a weaker-than-normal polar vortex in late winter can be induced by tropospheric stationary waves, which may reinforce vertical propagation of planetary-scale waves of wavenumber-1 that interfere with climatological waves.

Further analyses reveal that changes in large-scale atmospheric circulations in the troposphere (such as strengthening of the Ural blocking) are the main driver of the stratospheric polar vortex weakening in late winter. The temporal evolution in Figure 9 shows that the Ural pressure ridge changes from weaker-than-normal to stronger-than-normal state in late December–early January and intensifies thereafter, consistent with that in observations (Figure 4 and Figure S10 in Supporting Information S1). The development of the large-scale tropospheric ridge is followed by a deepened East Asian trough that occurred in late winter (Figure 9), forming the tropospheric planetary wave configuration that drives enhanced upward propagation of Rossby waves to weaken the polar vortex. This is consistent with Garfinkel et al. (2010), which indicates that the Ural blocking

10.1029/2022EF002790

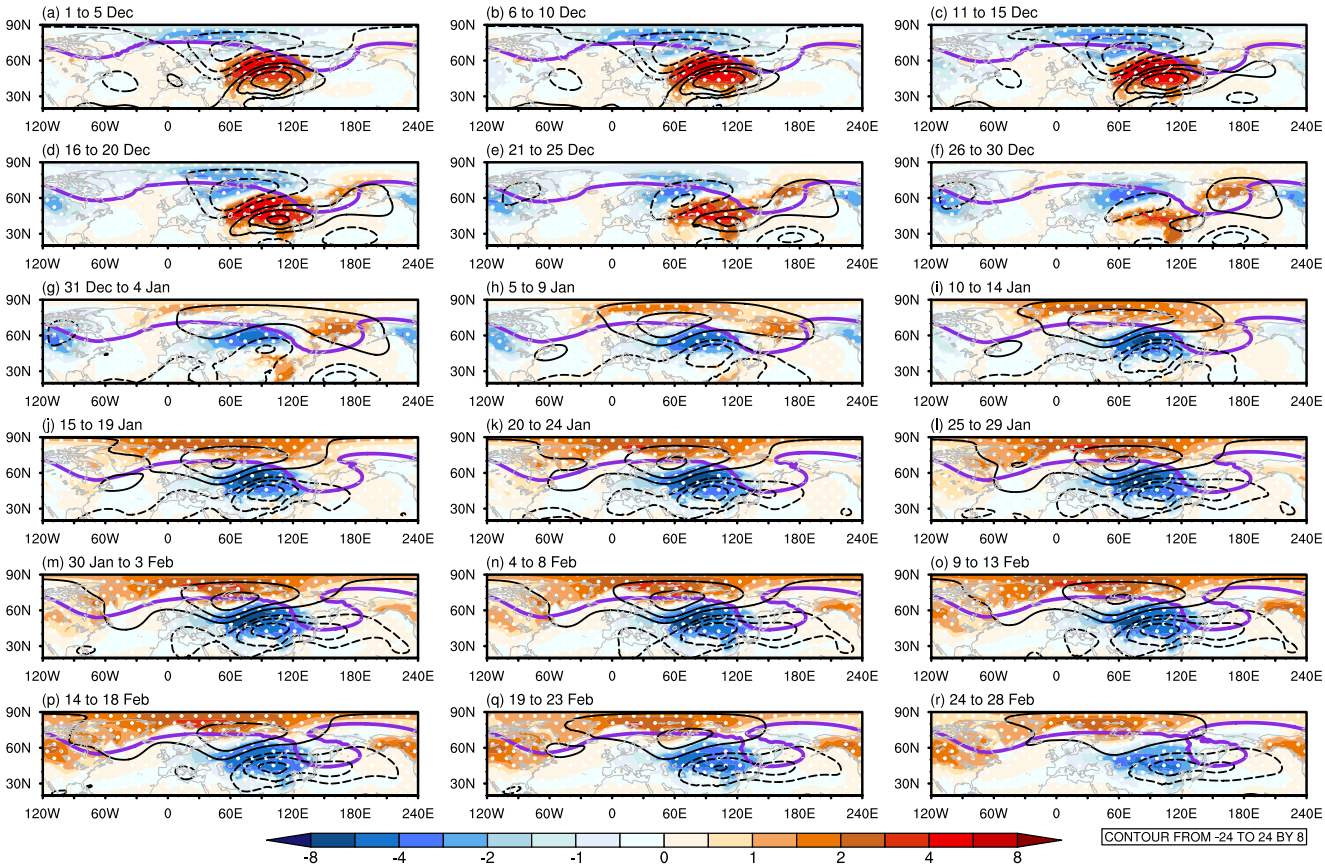

Figure 9. Differences of the 5-day averaged surface air temperature (shading; units: °C) and Z500 (black contours; units: m) anomalies composited between warm-to-cold and cold-to-warm winters over East Asia during 1920/1921–2099/2100 based on 40 ensemble members of Community Earth System Model Large Ensemble (CESM-LE). Regions with significant anomalies above the 95% confidence level are marked with dots. The black contours are displayed only if the corresponding anomalies exceed the 95% confidence level. Purple contours represent the climatological "isoheight" of 5200 gpm during 1920/1921–2099/2100 based on 40 ensemble members of CESM-LE.

development can be treated as a tropospheric precursor of the stratospheric polar vortex weakening. The weakened polar vortex in turn intensifies tropospheric circulation anomalies and causes reversed temperature anomalies in the Arctic-Eurasian regions.

4. Conclusions and Discussions

This study identifies the subseasonal reversal of SAT anomalies from early to late winter over the Arctic-Eurasian regions and explores its possible mechanisms based on the reanalysis data, the 1800-year CESM control simulation, and the 40-member ensemble of CESM-LE simulations for 1920–2100. Observational analyses show that approximately 45% of the winters experience a subseasonal reversal from significant warm (cold) anomalies in early winter to cold (warm) anomalies in late winter over Eurasia. Such reversals are associated with simultaneous yet opposite reversals of SAT anomalies over the Barents-Kara Seas. On the synoptic time scale, the reversal of SAT anomalies first emerges in the Arctic (i.e., warming over the Barents-Kara Seas) in late December and persists until February. A subsequent reversal of SAT anomalies occurs downstream from early January (i.e., colder Eurasia). Such a lagged and downstream reversal implies the potential effect of Arctic warming, which has been discussed in many studies (Kug et al., 2015; Mori et al., 2019), yet still remains a controversial issue in climate science community (J. Cohen et al., 2020). On the other hand, the reversal of SAT anomalies over the Arctic-Eurasian regions could also be a result of the same climate systems (e.g., large-scale atmospheric patterns). Further analyses reveal several dynamic processes that might be responsible for the subseasonal reversal of SAT anomalies. For example, accompanied with "colder Arctic, warmer Eurasia" in early winter and "warmer Arctic, colder Eurasia" in late winter, there is a significant anomalous cyclone over the Urals in

early winter, which turns into an anomalous anticyclone (i.e., strengthened Ural blocking) in late winter. On the synoptic time scale, the occurrence frequency of the instantaneous blocking events over northern Eurasia increases before the Arctic warming, implying the possible role the Ural blocking may play that leads to SAT anomaly reversals over the Arctic-Eurasian regions. The atmospheric circulation anomalies in the troposphere include the strengthening of the Ural blocking and corresponding deceleration of the midlatitude westerly winds. These atmospheric circulation anomalies can affect the upward propagation of planetary-scale waves (Cohen & Jones, 2011; Dickinson, 1968), which subsequently influences stratospheric polar vortex (Kim et al., 2014) that contributes to the reversal of SAT anomalies in late winter.

Results from the CESM PiCTL and CESM-LE simulations further confirm the robust role of internal atmospheric variability in causing the subseasonal reversal of SAT anomalies over the Arctic-Eurasian regions. The change from "colder Arctic, warmer Eurasia" in early (late) winter to "warmer Arctic, colder Eurasia" in late (early) winter can be detected in ~40% of winters simulated by the CESM PiCTL and CESM-LE. This sample proportion is close to that in reanalysis data (i.e., ~45%). Moreover, robust climate dynamic processes such as subseasonal reversals of anomalies in the Ural blocking, midlatitude westerly winds, and stratospheric polar vortex are in good accordance with those shown in reanalysis data. These results suggest that the internal atmospheric variability is an important factor that drives the subseasonal reversal of SAT anomalies. And the robust climate dynamics revealed by both reanalysis data and simulations indicate that the subseasonal reversal of SAT anomalies is one of the intrinsic and dominant features of the Arctic-Eurasian winter climate. Results from the CESM simulations further indicate that the perturbations of tropospheric atmospheric circulations such as wavenumber 1 disturbances might play an important role in triggering the troposphere-stratosphere interaction, which promotes the impacts of stratospheric polar vortex on the reversal of SAT anomalies in late winter. Previous studies have also suggested that the Ural blocking is a critical indicator for the subsequent planetary wave propagation (Cohen & Jones, 2011; Martius et al., 2009; Peings, 2019; Tyrlis et al., 2019). Therefore, the above results can provide some insights into the study for subseasonal predictability.

The role of Arctic sea ice decline is not considered here due to its undetermined impact on the upper tropospheric Arctic warming (J. Cohen et al., 2020) and anomalous downward turbulent heat flux from the atmosphere to the ocean (see Figure S6 in Supporting Information S1) (Blackport et al., 2019). Several recent studies suggested that the North Atlantic SST anomalies also play a crucial role in the reversal (Chen et al., 2020; Otomi et al., 2013) or persistence (Wu & Chen, 2020) of atmospheric circulations over Eurasia because the tropical North Atlantic SST anomalies can trigger an atmospheric wave train spanning from the North Atlantic to midlatitude Eurasia (Chen & Wu, 2017; Chen et al., 2018). Other tropical forcing can also contribute to the subseasonal variability of Eurasian climate (Agrawal et al., 2019; Matsumura & Kosaka, 2019). For example, the extensive irrigation-induced surface cooling over India in winter can modulate the intra-seasonal variability of Indian summer monsoon through inducing a positive NAO-like pattern (Agrawal et al., 2019). H. Li et al. (2021) revealed the intensified influence of Central Pacific ENSO on the reverse climate anomalies between December and January over China in recent decades. The comprehensive influences of background forcing (e.g., tropical forcing) and internal atmospheric variability on the subseasonal climate variability need to be further investigated by perturbed numerical simulations in the future. It is also noted that the sample proportions of reversal events are similar between historical simulations and future projections, implying that the internal mode is less likely to be influenced by climate change.

Data Availability Statement

The ERA-Interim data are available from https://www.ecmwf.int/en/forecasts/datasets/reanalysis-datasets/era-interim. The EAR20C data are available from https://apps.ecmwf.int/datasets/data/era20c-moda/levtype=sfc/type=an/. The 1800-year preindustrial control simulation and the 40-member ensemble long-term CESM-LE simulations are available from https://www.cesm.ucar.edu/experiments/cesm1.1/LE.

Acknowledgments
This research was supported by the National Natural Science Foundation of China (Grants No. 42088101, 42025502, and 41875118), the Research Council of Norway project BASIC (Grant No. 325440), and the State Scholarship Fund by China Scholarship Council (Grant No. 202109045003).

References

Agrawal, S., Arindam, C., Karmakar, N., Moulds, S., Mijic, A., & Buytaert, W. (2019). Effects of winter and summer-time irrigation over Gangetic Plain on the mean and intra-seasonal variability of Indian summer monsoon. *Climate Dynamics*, *53*(5–6), 3147–3166. https://doi.org/10.1007/s00382-019-04691-7

Andrews, D., Holton, J., & Leovy, C. (1987). *Middle atmosphere dynamics* (p. 489). Academic press.

Blackport, R., Screen, J. A., van der Wiel, K., & Bintanja, R. (2019). Minimal influence of reduced Arctic sea ice on coincident cold winters in mid-latitudes. *Nature Climate Change*, *9*, 697–704. https://doi.org/10.1038/s41558-019-0551-4

Chen, S., & Wu, R. (2017). Interdecadal changes in the relationship between interannual variations of spring North Atlantic SST and Eurasian surface air temperature. *Journal of Climate*, *30*(10), 3771–3787. https://doi.org/10.1175/jcli-d-16-0477.1

Chen, S., Wu, R., Chen, W., & Li, K. (2020). Why does a colder (warmer) winter tend to be followed by a warmer (cooler) summer over northeast Eurasia? *Journal of Climate*, *33*(17), 7255–7274. https://doi.org/10.1175/jcli-d-20-0036.1

Chen, S., Wu, R., Chen, W., & Yao, S. (2018). Enhanced linkage between Eurasian winter and spring dominant modes of atmospheric interannual variability since the early 1990s. *Journal of Climate*, *31*(9), 3575–3595. https://doi.org/10.1175/jcli-d-17-0525.1

Cheung, H. H. N., Zhou, W., Leung, M. T., Shun, C. M., Lee, S. M., & Tong, H. W. (2016). A strong phase reversal of the Arctic Oscillation in midwinter 2015/2016: Role of the stratospheric polar vortex and tropospheric blocking. *Journal of Geophysical Research: Atmosphere*, *121*(22), 13443–13457. https://doi.org/10.1002/2016jd025288

Cohen, J., & Jones, J. (2011). Tropospheric precursors and stratospheric warmings. *Journal of Climate*, *24*, 6562–6572. https://doi.org/10.1175/2011jcli4160.1

Cohen, J., Screen, J. A., Furtado, J. C., Barlow, M., Whittleston, D., Coumou, D., et al. (2014). Recent Arctic amplification and extreme mid-latitude weather. *Nature Geoscience*, *7*(9), 627–637. https://doi.org/10.1038/ngeo2234

Cohen, J., Zhang, X., Francis, J., Jung, T., Kwok, R., Overland, J., et al. (2020). Divergent consensuses on Arctic amplification influence on midlatitude severe winter weather. *Nature Climate Change*, *10*(1), 20–29. https://doi.org/10.1038/s41558-019-0662-y

Cohen, J. L., Furtado, J. C., Barlow, M. A., Alexeev, V. A., & Cherry, J. E. (2012). Arctic warming, increasing snow cover and widespread boreal winter cooling. *Environmental Research Letters*, *7*(1), 014007. https://doi.org/10.1088/1748-9326/7/1/014007

Cowtan, K., & Way, R. G. (2013). Coverage bias in the HadCRUT4 temperature series and its impact on recent temperature trends. *Quarterly Journal of the Royal Meteorological Society*, *133*, 459–477. https://doi.org/10.1002/qj.2297

Dai, H., Fan, K., & Liu, J. (2019). Month-to-month variability of winter temperature over Northeast China linked to sea ice over the Davis Strait–Baffin Bay and the Barents–Kara Sea. *Journal of Climate*, *32*(19), 6365–6384. https://doi.org/10.1175/jcli-d-18-0804.1

Dee, D. P., Uppala, S. M., Simmons, A. J., Berrisford, P., Poli, P., Kobayashi, S., et al. (2011). The ERA-interim reanalysis: Configuration and performance of the data assimilation system. *Quarterly Journal of the Royal Meteorological Society*, *137*(656), 553–597. https://doi.org/10.1002/qj.828

Deser, C., Terray, L., & Phillips, A. S. (2016). Forced and internal components of winter air temperature trends over North America during the past 50 years: Mechanisms and implications. *Journal of Climate*, *29*(6), 2237–2258. https://doi.org/10.1175/jcli-d-15-0304.1

Dickinson, R. E. (1968). Planetary Rossby waves propagating vertically through weak westerly wind wave guides. *Journal of the Atmospheric Sciences*, *25*(6), 984–1002. https://doi.org/10.1175/1520-0469(1968)025<0984:prwpvt>2.0.co;2

Furtado, J. C., Cohen, J. L., Butler, A. H., Riddle, E. E., & Kumar, A. (2015). Eurasian snow cover variability and links to winter climate in the CMIP5 models. *Climate Dynamics*, *45*(9–10), 1–15. https://doi.org/10.1007/s00382-015-2494-4

Gao, Y., Sun, J., Li, F., He, S., Sandven, S., Yan, Q., et al. (2015). Arctic sea ice and Eurasian climate: A review. *Advances in Atmospheric Sciences*, *32*(1), 92–114. https://doi.org/10.1007/s00376-014-0009-6

Garfinkel, C. I., Hartmann, D. L., & Sassi, F. (2010). Tropospheric precursors of anomalous Northern Hemisphere stratospheric polar vortices. *Journal of Climate*, *23*(12), 3282–3299. https://doi.org/10.1175/2010jcli3010.1

Geng, X., Zhang, W., Stuecker, M. F., & Jin, F.-F. (2017). Strong sub-seasonal wintertime cooling over East Asia and Northern Europe associated with super El Niño events. *Scientific Reports*, *7*(1), 3770. https://doi.org/10.1038/s41598-017-03977-2

He, S., & Wang, H. (2013). Impact of the November/December Arctic Oscillation on the following January temperature in East Asia. *Journal of Geophysical Research: Atmospheres*, *118*(23), 12981–12998. https://doi.org/10.1002/2013jd020525

He, S., Wang, H., Xu, X., & Li, J. (2016). Impact of Arctic warming and the super El Niño in winter 2015/2016 on the East Asian climate anomaly. *Transactions of Atmospheric Sciences*, *39*, 735–743. (in Chinese).

He, S., Xu, X., Furevik, T., & Gao, Y. (2020). Eurasian cooling linked to the vertical distribution of Arctic warming. *Geophysical Research Letters*, *47*(10), e2020GL087212. https://doi.org/10.1029/2020gl087212

Huang, J., Hitchcock, P., Maycock, A. C., Mckenna, C. M., & Tian, W. (2021). Northern Hemisphere cold air outbreaks are more likely to be severe during weak polar vortex conditions. *Communications Earth & Environment*, *2*(1), 147. https://doi.org/10.1038/s43247-021-00215-6

Kay, J. E., Deser, C., Phillips, A., Mai, A., Hannay, C., Strand, G., et al. (2015). The Community Earth System Model (CESM) large ensemble project: A community resource for studying climate change in the presence of internal climate variability. *Bulletin of the American Meteorological Society*, *96*(8), 1333–1349. https://doi.org/10.1175/bams-d-13-00255.1

Kim, B.-M., Hong, J. Y., Jun, S. Y., Zhang, X., Kwon, H., Kim, S. J., et al. (2017). Major cause of unprecedented Arctic warming in January 2016: Critical role of an Atlantic windstorm. *Scientific Reports*, *7*(1), 40051. https://doi.org/10.1038/srep40051

Kim, B. M., Son, S. W., Min, S. K., Jeong, J. H., Kim, S. J., Zhang, X., et al. (2014). Weakening of the stratospheric polar vortex by Arctic sea-ice loss. *Nature Communications*, *5*(1), 4646. https://doi.org/10.1038/ncomms5646

King, M. P., Herceg-Bulić, I., Bladé, I., García-Serrano, J., Keenlyside, N., Kucharski, F., et al. (2018). Importance of late fall ENSO teleconnection in the Euro-Atlantic sector. *Bulletin of the American Meteorological Society*, *99*(7), 1337–1343. https://doi.org/10.1175/bams-d-17-0020.1

King, M. P., Li, C., & Sobolowski, S. (2021). Resampling of ENSO teleconnections: Accounting for cold season evolution reduces uncertainty in the North Atlantic. *Weather and Climate Dynamics*, *2*(3), 759–776. https://doi.org/10.5194/wcd-2-759-2021

Kug, J. S., Jeong, J. H., Jang, Y. S., Kim, B. M., Folland, C. K., Min, S. K., & Son, S. W. (2015). Two distinct influences of Arctic warming on cold winters over North America and East Asia. *Nature Geoscience*, *8*(10), 759–762. https://doi.org/10.1038/ngeo2517

Labe, Z., Peings, Y., & Magnusdottir, G. (2020). Warm Arctic, cold Siberia pattern: Role of full Arctic amplification versus sea ice loss alone. *Geophysical Research Letters*, *47*(17), e2020GL088583. https://doi.org/10.1029/2020gl088583

Li, H., Fan, K., He, S., Liu, Y., Yuan, X., & Wang, H. (2021). Intensified impacts of central Pacific ENSO on the reversal of December and January surface air temperature anomaly over China since 1997. *Journal of Climate*, *34*(5), 1601–1618. https://doi.org/10.1175/jcli-d-20-0048.1

Li, S., He, S., Li, F., & Wang, H. (2018). Simulated and projected relationship between the East Asian winter monsoon and winter Arctic Oscillation in CMIP5 models. *Atmospheric and Oceanic Science Letters*, *11*(5), 417–424. https://doi.org/10.1080/16742834.2018.1512356

Liu, J., Curry, J. A., Wang, H., Song, M., & Horton, R. M. (2012). Impact of declining Arctic sea ice on winter snowfall. *Proceedings of the National Academy of Sciences of the United States of America*, *109*(11), 4074–4079. https://doi.org/10.1073/pnas.1114910109

Luo, D., Xiao, Y., Yao, Y., Dai, A., Simmonds, I., & Franzke, C. L. E. (2016). Impact of Ural blocking on winter warm Arctic-cold Eurasian anomalies. Part I: Blocking-induced amplification. *Journal of Climate*, *29*(11), 3925–3947. https://doi.org/10.1175/jcli-d-15-0611.1

Martius, O., Polvani, L. M., & Davies, H. C. (2009). Blocking precursors to stratospheric sudden warming event. *Geophysical Research Letters*, *36*(14), L14806. https://doi.org/10.1029/2009gl038776

Matsumura, S., & Kosaka, Y. (2019). Arctic-Eurasian climate linkage induced by tropical ocean variability. *Nature Communications*, *10*(1), 3441. https://doi.org/10.1038/s41467-019-11359-7
McCusker, K. E., Fyfe, J. C., & Sigmond, M. (2016). Twenty-five winters of unexpected Eurasian cooling unlikely due to Arctic sea-ice loss. *Nature Geoscience*, *9*(11), 838–842. https://doi.org/10.1038/ngeo2820
Miao, J., Wang, T., & Wang, H. (2019). Interdecadal variations of the East Asian winter monsoon in CMIP5 preindustrial simulations. *Journal of Climate*, *33*(2), 559–575. https://doi.org/10.1175/jcli-d-19-0148.1
Mori, M., Kosaka, Y., Watanabe, M., Nakamura, H., & Kimoto, M. (2019). A reconciled estimate of the influence of Arctic sea-ice loss on recent Eurasian cooling. *Nature Climate Change*, *9*(2), 123–129. https://doi.org/10.1038/s41558-018-0379-3
Orsolini, Y. J., & Kvamstø, N. G. (2009). Role of Eurasian snow cover in wintertime circulation: Decadal simulations forced with satellite observations. *Journal of Geophysical Research*, *114*(D19), D19108. https://doi.org/10.1029/2009jd012253
Otomi, Y., Tachibana, Y., & Nakamura, T. (2013). A possible cause of the AO polarity reversal from winter to summer in 2010 and its relation to hemispheric extreme summer weather. *Climate Dynamics*, *40*(7–8), 1939–1947. https://doi.org/10.1007/s00382-012-1386-0
Overland, J., Francis, J. A., Hall, R., Hanna, E., Kim, S. J., & Vihma, T. (2015). The melting Arctic and midlatitude weather patterns: Are they connected? *Journal of Climate*, *28*(20), 7917–7932. https://doi.org/10.1175/jcli-d-14-00822.1
Overland, J. E., Wood, K. R., & Wang, M. (2011). Warm Arctic-cold continents: Climate impacts of the newly open Arctic sea. *Polar Research*, *30*(1), 157–171. https://doi.org/10.3402/polar.v30i0.15787
Peings, Y. (2019). Ural blocking as a driver of early-winter stratospheric warmings. *Geophysical Research Letters*, *46*(10), 5460–5468. https://doi.org/10.1029/2019gl082097
Peings, Y., & Magnusdottir, G. (2014). Response of the wintertime Northern Hemisphere atmospheric circulation to current and projected Arctic sea ice decline: A numerical study with CAM5. *Journal of Climate*, *27*(1), 244–264. https://doi.org/10.1175/jcli-d-13-00272.1
Poli, P., Hersbach, H., Dee, D. P., Berrisford, P., Simmons, A. J., Vitart, F., et al. (2016). ERA-20C: An atmospheric reanalysis of the twentieth century. *Journal of Climate*, *29*(11), 4083–4097. https://doi.org/10.1175/jcli-d-15-0556.1
Polvani, L. M., & Waugh, D. W. (2004). Upward wave activity flux as a precursor to extreme stratospheric events and subsequent anomalous surface weather regimes. *Journal of Climate*, *17*(18), 3548–3554. https://doi.org/10.1175/1520-0442(2004)017<3548:uwafaa>2.0.co;2
Rayner, N. A., Parker, D. E., Horton, E. B., Folland, C. K., Alexander, L. V., Rowell, D. P., et al. (2003). Global analyses of sea surface temperature, sea ice, and night marine air temperature since the late nineteenth century. *Journal of Geophysical Research*, *108*(D14), 1063–1082. https://doi.org/10.1029/2002jd002670
Screen, J. A. (2017). Far-flung effects of Arctic warming. *Nature Geoscience*, *10*(4), 253–254. https://doi.org/10.1038/ngeo2924
Screen, J. A., Deser, C., Smith, D. M., Zhang, X., Blackport, R., Kushner, P. J., et al. (2018). Consistency and discrepancy in the atmospheric response to Arctic sea-ice loss across climate models. *Nature Geoscience*, *11*(3), 155–163. https://doi.org/10.1038/s41561-018-0059-y
Screen, J. A., & Simmonds, I. (2010). The central role of diminishing sea ice in recent Arctic temperature amplification. *Nature*, *464*(7293), 1334–1337. https://doi.org/10.1038/nature09051
Sorokina, S. A., Li, C., Wettstein, J. J., & Kvamstø, N. G. (2016). Observed atmospheric coupling between Barents Sea ice and the warm-Arctic cold-Siberian anomaly pattern. *Journal of Climate*, *29*(2), 495–511. https://doi.org/10.1175/jcli-d-15-0046.1
Sung, M.-K., Kim, S.-H., Kim, B.-M., & Choi, Y.-S. (2018). Interdecadal variability of the warm Arctic and cold Eurasia pattern and its North Atlantic origin. *Journal of Climate*, *31*(15), 5793–5810. https://doi.org/10.1175/jcli-d-17-0562.1
Tao, S., & Chen, L. (1987). A review of recent research of the east Asian summer monsoon in China. In C. P. Change & T. N. Krishnamurti (Eds.), *Monsoon meteorology* (pp. 60–92). Oxford University Press.
Tibaldi, S., & Molteni, F. (1990). On the operational predictability of blocking events. *Tellus*, *42*(3), 343–365. https://doi.org/10.1034/j.1600-0870.1990.t01-2-00003.x
Tyrlis, E., Manzini, E., Bader, J., Ukita, J., Nakamura, H., & Matei, D. (2019). Ural blocking driving extreme Arctic sea ice loss, cold Eurasia, and stratospheric vortex weakening in autumn and early winter 2016-2017. *Journal of Geophysical Research: Atmospheres*, *124*(21), 11313–11329. https://doi.org/10.1029/2019jd031085
Vavrus, S. J. (2018). The influence of Arctic amplification on mid-latitude weather and climate. *Current Climate Change Reports*, *4*(3), 238–249. https://doi.org/10.1007/s40641-018-0105-2
Wang, B., Wu, R., & Fu, X. (2000). Pacific-East Asian teleconnection: How does ENSO affect East Asian climate? *Journal of Climate*, *13*(9), 1517–1536. https://doi.org/10.1175/1520-0442(2000)013<1517:peathd>2.0.co;2
Wang, H., Chen, H., & Liu, J. (2015). Arctic sea ice decline intensified haze pollution in eastern China. *Atmospheric and Oceanic Science Letters*, *8*, 1–9. https://doi.org/10.3878/AOSL20140081
Wang, H., & He, S. (2012). Weakening relationship between East Asian winter monsoon and ENSO after mid-1970s. *Chinese Science Bulletin*, *57*(27), 3535–3540. https://doi.org/10.1007/s11434-012-5285-x
Wang, L., Huang, R., Gu, L., Chen, W., & Kang, L. (2009). Interdecadal variations of the East Asian winter monsoon and their association with quasi-stationary planetary wave activity. *Journal of Climate*, *22*(18), 4860–4872. https://doi.org/10.1175/2009jcli2973.1
Wang, S., & Liu, J. (2016). Delving into the relationship between autumn Arctic sea ice and central-eastern Eurasian winter climate. *Atmospheric and Oceanic Science Letters*, *9*(5), 366–374. https://doi.org/10.1080/16742834.2016.1207482
Wu, R., & Chen, S. (2020). What leads to persisting surface air temperature anomalies from winter to following spring over the mid-high latitude Eurasia? *Journal of Climate*, *33*(14), 5861–5883. https://doi.org/10.1175/jcli-d-19-0819.1
Xu, X., He, S., Li, F., & Wang, H. (2018). Impact of northern Eurasian snow cover in autumn on the warm Arctic-cold Eurasia pattern during the following January and its linkage to stationary planetary waves. *Climate Dynamics*, *50*(5–6), 1993–2006. https://doi.org/10.1007/s00382-017-3732-8
Xu, X., Li, F., He, S., & Wang, H. (2018). Sub-seasonal reversal of East Asian surface temperature variability in winter 2014/2015. *Advances in Atmospheric Sciences*, *35*(6), 737–752. https://doi.org/10.1007/s00376-017-7059-5
Ye, K., Jung, T., & Semmler, T. (2018). The influences of the Arctic troposphere on the midlatitude climate variability and the recent Eurasian cooling. *Journal of Geophysical Research: Atmospheres*, *123*(18), 10162–10184. https://doi.org/10.1029/2018jd028980
Zhang, G., Gao, Y., Cai, W., Leung, L. R., Wang, S., Zhao, B., et al. (2019). Seesaw haze pollution in North China modulated by the sub-seasonal variability of atmospheric circulation. *Atmospheric Chemistry and Physics*, *19*(1), 565–576. https://doi.org/10.5194/acp-19-565-2019
Zhang, Y., Sperber, K. R., & Boyle, J. S. (1997). Climatology and interannual variation of the East Asian winter monsoon: Results from the 1979-95 NCEP/NCAR reanalysis. *Monthly Weather Review*, *125*(10), 2605–2619. https://doi.org/10.1175/1520-0493(1997)125<2605:caivot>2.0.co;2